Available online at www.sciencedirect.com
SCIENCE DIRECT®
Journal of Power Sources 129 (2004) 280–287
JOURNAL OF POWER SOURCES
www.elsevier.com/locate/jpowsour

Increased lithium-ion conductivity in $(PEG)_{46}LiClO_4$ solid polymer electrolyte with δ-Al_2O_3 nanoparticles

Th. Joykumar Singh, S.V. Bhat*

Department of Physics, Indian Institute of Science, Bangalore 560012, India

Received 6 August 2003; accepted 5 November 2003

Abstract

The effect of δ-Al_2O_3 nanoparticles (size ∼ 10 nm) on the ionic conductivity and related properties of a solid polymer electrolyte (SPE) that consists of low molecular weight ($M_w = 2000$) poly(ethylene) glycol (PEG) complexed with $LiClO_4$ is studied in detail using XRD, DSC, TPD, NMR, and complex impedance methods. The maximum ionic conductivity $\sigma = 7.3 \times 10^{-7}$ S cm^{-1} observed for pristine $(PEG)_{46}LiClO_4$ is found to be dependent on the content of δ-Al_2O_3 filter; it shows a peak value of $\sigma = 4.5 \times 10^{-6}$ S cm^{-1} for 10 mol% filler. This is nearly an order of magnitude enhancement of the ionic conductivity and is found by DSC studies to be related to a decrease in the crystalline regions in the SPE, while the glass transition temperature T_g and the melting temperature T_m remain essentially unchanged. ^{7}Li NMR motional narrowing points to an increase in the effective mobility of the lithium ions on doping with the nanoparticles. The temperature dependence of σ can be divided into two regions, one consistent with the Arrhenius behavior and the other with the Vogel, Tamman and Fulcher equation. The activation energy is found to be the lowest for the 10 mol% doped sample. It is concluded that doping with nanoparticles leads to an enhancement of conductivity due to a decrease in the crystallinity and the activation energy, as well as to an increase in the effective mobility of Li ions.

Keywords: Nanocomposite polymer electrolyte; Ionic conductivity; Acidic δ-Al_2O_3; Glass transition temperature; ^{7}Li NMR

1. Introduction

Polyether based solid polymer electrolytes (SPEs) doped with lithium salts have been studied intensely in recent years. This interest is stimulated by possible applications in batteries with high specific energy, electrochromic displays, sensors, and fuel cells [1]. Compared with glassy and inorganic crystalline counterparts, SPEs have important advantages such as easier fabrication, mechanical flexibility, and corrosion resistance. Nevertheless, SPEs have certain technical limitations; the more serious are low ionic conductivity, high crystallinity, low transference number for cations, and poor mechanical stability. One of the more promising approaches to overcoming these problems has been to add inorganic electrically inert fillers to produce composite polymer electrolytes (CPEs). Beginning with the first study by Weston and Steele [2], which reported an improvement in the mechanical property of $(PEO)_8LiClO_4$ on doping with α-alumina powder of 40 μm size, many workers have investigated CPEs. It has been found that, in addition to an improvement in mechanical properties, doping with inorganic fillers such as Al_2O_3, TiO_2, SiO_2, zeolites, γ-$LiAlO_4$ and $BaTiO_3$ also causes an enhancement in ionic conductivity [3–8].

Recent studies have shown that the particle size and the nature of the fillers have an important influence on the enhancement of ionic conductivity; usually, the smaller the size the larger is the enhancement. In particular, fillers with nanosize particles are very effective in this regard [4,9]. Despite the numerous studies of such nanocomposite polymer electrolytes (NCPEs), the role played by the nanoparticles in the enhancement of ionic conductivity is not yet fully understood. For example, it is generally observed that the introduction of nanoparticles into a biphasic SPE (i.e., consisting of both crystalline and amorphous regions) leads to a decrease in the crystalline regions in the material. Since ionic conductivity takes place mostly in the amorphous regions of the SPEs, this reduction in the crystalline regions is expected to lead to an increase in the ionic conductivity. It is also recognized, however, that a decrease in crystallinity is not the only effect of the addition of the nanoparticles. For example, there have been conflicting reports on the effect of nanoparticles on the glass transition temperature

* Corresponding author. Tel.: +91-80-293-2727; fax: +91-80-360-2602.
E-mail address: svbhat@physics.iisc.emet.in (S.V. Bhat).

0378-7753/$ – see front matter © 2003 Elsevier B.V. All rights reserved.
doi:10.1016/j.jpowsour.2003.11.025

T_g. While no appreciable change in T_g was observed for $(PEO)_8LiBF_4 + 10$ wt.% Al_2O_3 (13 nm) [9], a decrease in T_g was seen for a $(PEO)_{16}LiClO_4 + 10$ wt.% Al_2O_3 (37 nm) NCPE system [10]. In $(PEG)_8$LiTFSI doped with nanoscale SiO_2, T_g was found to increase by a few degrees [11]. Moreover, the nature of the role played by the nanoparticles in modifying the properties of the SPE is yet to be clarified. So far, different mechanisms of interactions have been proposed such as an increase in the disorder of the system [11,12], Lewis acid–base type interactions of fillers with the salt or the polymer [13], increase in ionic mobility [14,15], increase in transference number [4], increased segmental motion of host polymer [10], electrostatic interactions between ionic species and fillers [16], space charge formation [17], and creation of new favorable conduction pathways [14].

It is known that polymers below a critical molecular weight (∼3200) display different viscosity and diffusion behavior. A study of the effect of molecular weight of polymer on cation mobility by Shi and Vincent [18] has shown that even though the molecular weight has no significant effect on cation mobility above a critical limit of 3200, an additional cation transport mechanism could be operating below this limit. In this low molecular weight region, referred to as the Rouse region, there is a possibility of polymer chain diffusion in addition to segmental motion. Accordingly, this study examines a new solid polymer electrolyte based on poly(ethylene) glycol (PEG) of molecular weight 2000 complexed with lithium perchlorate. Lithium perchlorate is chosen as it fulfils the electrochemical stability criteria and it has a low lattice energy (723 kJ mol^{-1}), which is favorable for polymer–salt complex formation. While there have been reports of the influence of γ- and α-Al_2O_3 nanoparticles on SPEs, and it is known that different alumina nanoparticles have different effects [11,13,19], the influence of doping with δ-Al_2O_3 nanoparticles has still to be examined. In the present work, detailed conductivity, DSC, XRD, and NMR studies of the $(PEG)_{46}LiClO_4 + $ δ-Al_2O_3 polymer electrolyte nanocomposite system are reported. It has been shown earlier that the $(PEG)_xLiClO_4$ SPE system has maximum ionic conductivity for $x = 46$ [20].

2. Experimental

Poly(ethylene) glycol of molecular weight 2000 (Fluka) and $LiClO_4$ (Fluka) were used without further purification. The nanoparticles used in the study were provided by Nanopowder Enterprises Inc., USA. XRD (Scintag XDS2000, USA) and TEM (JEOL, JEM 200CX) measurements were carried out to determine the size and shape of these nanoparticles. $LiClO_4$ was dried in an oven overnight at 100–110 °C prior to use. The ceramic filler was also dried in the oven at around 110 °C for 24–30 h. The sample was prepared by the solution casting method and using methanol (20–30 ml, analytical grade) as the common solvent. The nanoparticles were introduced into the complex solution of $(PEG)_{46}LiClO_4$. Sonication using high intensity ultrasonic vibration (Vibra Cell, Sonics and Materials, USA) with the finger directly immersed in the solution was performed for 1 h to ensure uniform dispersion of the nanoparticles into the polymer–salt matrix. The slurry was then stirred with a magnetic stirrer for 6 h at room temperature, followed by another hour at ∼50 °C in a nitrogen atmosphere. This facilitated the evaporation of the major part of the solvent. The viscous slurry was then poured into Teflon rings and kept in a glove box under nitrogen atmosphere overnight and the solvent was allowed to evaporate slowly. The solidified sample was transferred to a vacuum desiccator for drying under continuous pumping for 3 h to remove any traces of solvent present in the samples.

DSC measurements were carried out on MDSC 2920 equipment (TA Instruments, USA) in the standard mode with dry nitrogen gas purging at a rate of 25 ml min^{-1}. Ten to l2 mg of the sample was used for DSC measurements. Samples were heated to 100 °C at a rate of 5 °C min^{-1}, cooled to −100 °C, and then heated again. An empty aluminum pan was used as a reference.

Conductivity experiments were carried out in dry nitrogen atmosphere. The sample was loaded into a cell with a pair of spring-fit, stainless-steel, blocking electrodes. Impedance measurements were carried out with a 0.5 V ac signal by means of a PAR 5210 vector lock-in amplifier in the frequency range 2 Hz to 120 kHz. Measurements were conducted every 5 °C during heating using a Bruker VT-1000 temperature controller. After the desired temperature was reached, the sample was allowed to equilibrate for 20–25 min before a reading was taken. The experiments were carried out in the temperature range of 260–340 K. All the experimental spectra were analyzed by means of the Boukamp Equivalent Circuit method [21].

3. Results and discussion

3.1. Shape and size of nanoparticles

The X-ray diffraction pattern of the nanoparticles was recorded at a scan rate of 10° min^{-1} to determine the size of the crystallites in the nanoparticles. The pattern is very similar to that reported for δ-Al_2O_3 [22,23]. Hereafter, the nanoparticles used in the present studies are referred to as δ-Al_2O_3. The two most intense XRD peaks (Fig. 1) were chosen for calculation of nanoparticle size. The diameter of the δ-Al_2O_3 nanoparticles, L, was calculated from the full width at half maxima (FWHM), Γ, expressed in radians, of the XRD peaks using Scherrer's equation [24,25] $\Gamma = 0.94\lambda/(L\cos\theta)$, where θ is the diffraction peak position. L was found to be ∼7 nm. Application of the Scherrer formula leads to an estimate of the mean crystallite size. TEM imaging was also carried out (Fig. 2) to determine the shape and size of the particles and an average size of ∼12 nm was

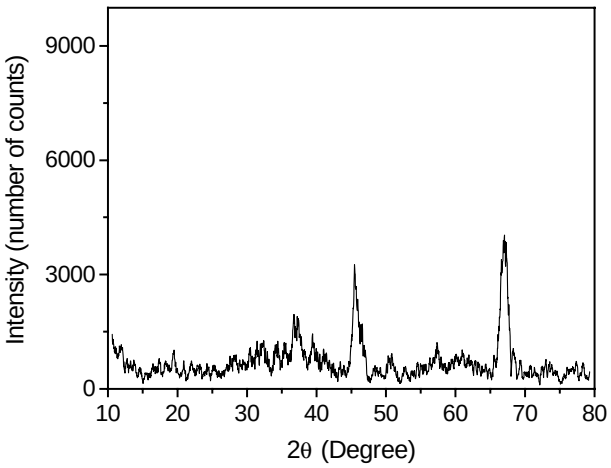

Fig. 1. XRD pattern of δ-alumina nanoparticles.

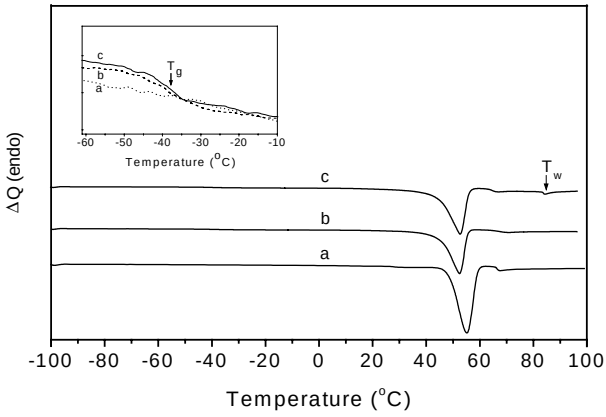

Fig. 3. DSC results for: (a) pure PEG 2000, (b) $(PEG)_{46}LiClO_4$, and (c) $(PEG)_{46}LiClO_4 + \delta\text{-}Al_2O_3$ (10 mol%). Inset shows relevant regions magnified.

obtained. It is to be noted that Scherrer analysis of the XRD pattern gives crystallite size and not particle size. Nanoparticles are expected to be mostly single-crystalline and therefore the size observed is very nearly that of the particle size itself. Understandably, this technique has been widely used by other workers to determine the size of the nanoparticles [24,25]. The fact that the value obtained by TEM is of the same order of magnitude as that obtained from XRD also lends credence to this conclusion. The particles are essentially spherical in shape. Nanoparticles of this size are particularly useful as fillers in the SPE, since it has been shown [9] that smaller particle size gives rise to more enhancement in conductivity.

3.2. Thermal properties

The DSC curves for pure PEG 2000, SPE $(PEG)_{46}LiClO_4$ and NCPE with maximum ionic conductivity $(PEG)_{46}LiCO_4 + \delta\text{-}Al_2O_3$ (10 mol%) are shown in Fig. 3. Curves for other compositions (not shown) are similar to those of the 10 mol% composition. All the SPE samples exhibit a relatively sharp endothermic peak near 52 °C, which could be attributed to the melting of a PEG-rich crystalline phase. Noteworthy is the observation that the dispersion of the nanoparticles does not alter this melting temperature T_m.

The area under the curve of the melting endotherm, which gives the latent heat of melting, ΔQ_m, is found to be dependent on the composition of the specimen. As is well known, the % crystallinity (X_c) of the sample can be obtained by comparing the heat of melting ΔQ_m with that of a sample of known % crystallinity. From NMR measurements, pure PEG 2000 has been found to be 83% crystalline [26]. The percentage crystallinity of $(PEG)_{46}LiClO_4 + \delta\text{-}Al_2O_3$ for different nanoparticle contents obtained by comparing their heats of melting with that of pure PEG is presented in Table 1 and also plotted in Fig. 4. It is noted that the ΔQ_m

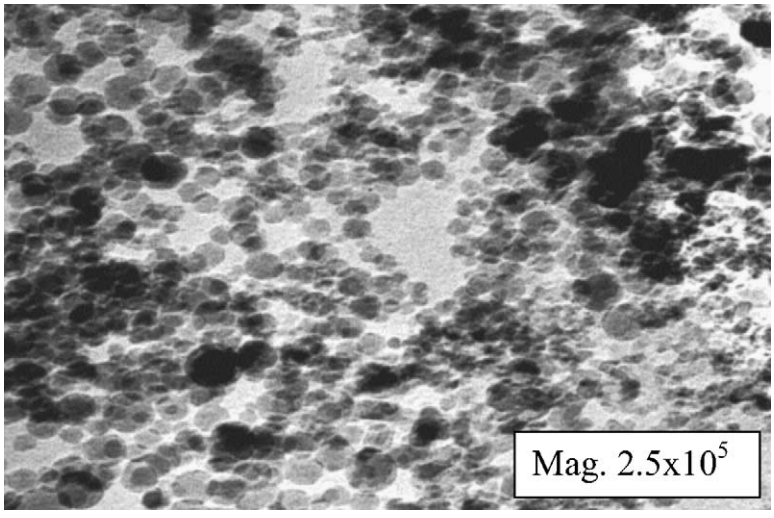

Fig. 2. TEM image of δ-alumina nanoparticles.

Table 1
DSC results

Sample	δ-Al_2O_3 (mol%)	ΔH (J g^{-1})	T_m (°C)	T_g (°C)
PEG	–	168.0	55.2	–
$(PEG)_{46}LiClO_4$	–	142.4	52.3	−38.8 ± 1.0
$(PEG)_{46}LiClO_4$	5	124.7	52.3	−39.1 ± 1.0
$(PEG)_{46}LiClO_4$	10	125.9	52.8	−36.7 ± 1.0
$(PEG)_{46}LiClO_4$	15	127.8	52.6	−36.9 ± 1.0
$(PEG)_{46}LiClO_4$	25	132.8	52.4	−37.4 ± 1.0
$(PEG)_{46}LiClO_4$	30	127.6	52.2	−37.9 ± 1.0

obtained from the DSC curves for any given composition is reproducible to within ±1.5%. The % crystallinity is the ratio of two such ΔQ_m s and it is estimated that X_c values are correct to within ±3%. The error bars corresponding to this experimental uncertainty are shown on the data points in Fig. 4. It is seen that on the introduction of the nanoparticles, the crystallinity of the SPE falls sharply from ∼70% for samples with no filler to 62% for 5–10 mol% filler. For higher contents of nanoparticles, X_c is seen to be independent of the composition within the experimental error.

A weaker second peak is observed for pure PEG 2000 in the second heating cycle. This could be due to the segregation of two types of crystalline regions after the first heating and cooling cycle. Further studies have to be conducted to confirm this suggestion. It is also observed that for the SPE and composites filled with nanoparticles another weak endotherm (marked by an arrow in Fig. 3) appears at a temperature $T_w > T_m$. Such additional endotherms have been observed [27] in many systems such as PEO–$LiFCl_3SO_3$ and PEO + NaSCN and have usually been attributed to the melting/dissolution process of a salt-rich crystalline phase.

The glass transition temperature T_g cannot be observed for pure PEG, most probably due to its highly crystalline nature. After complexation with $LiClO_4$, the SPE exhibits a T_g at nearly −39 °C. Successive measurements and analysis show that this value can be reproduced within ±1 °C. It is

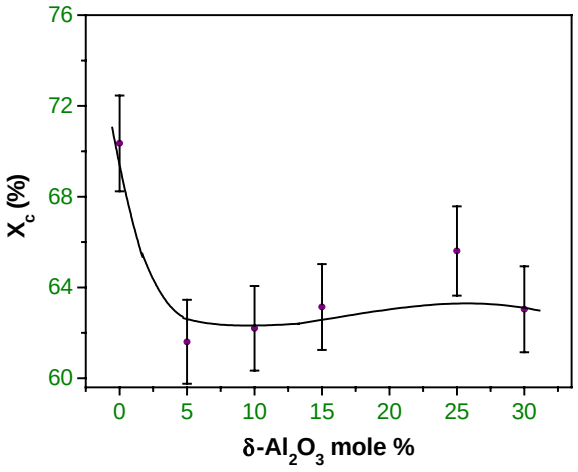

Fig. 4. Degree of crystallinity vs. δ-Al_2O_3 (mol%) plot for $(PEG)_{46}LiClO_4$ + δ-Al_2O_3. Solid line (—) is a guide to the eye.

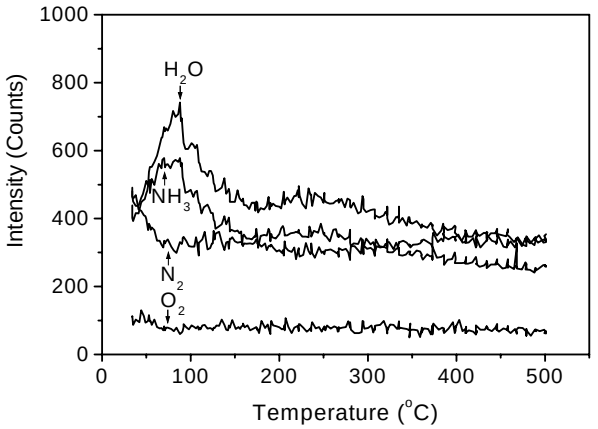

Fig. 5. Thermogram plots of NH_3, H_2O, O_2 and N_2.

seen from this that on the addition of δ-Al_2O_3 nanoparticles there is no appreciable change in T_g. Similar observations have been made by other workers in similar systems [9,14].

3.3. Temperature-programmed desorption (TPD) studies

The δ-Al_2O_3 nanoparticles could have on their surface either Lewis base centers or Lewis acid centers or the surface could be neutral. It has been reported that the nature of the surface has significant effect on the conductivity [11,13,19]. To determine the nature of the surface groups, temperature-programmed desorption studies were carried out with a quadrupole mass spectrometer QXK300 (VG Scientific Limited, UK). Typically, 0.05 mg of δ-Al_2O_3 nanoparticles was loaded in a quartz tube reactor of 20 cm length and 6 mm diameter. The quartz tube was evacuated to 10^{-6} Torr. Then, it was saturated with 4.6% NH_3 in He (calibration gas mixture from Bhoruka Gases Ltd., Bangalore) for 30 min. This was followed by evacuation of the tube and then TPD was carried out at a heating rate of 10 °C min^{-1} from 30 to 500 °C. The sample temperature was measured by a fine chromel–alumel thermocouple immersed in the catalyst. The desorbing gas products were leaked into an ultra high vacuum system that housed the quadrupole mass spectrometer at $l0^{-9}$ Torr. All the masses were scanned every 10 s. The intensity of each species of H_2O, NH_3, O_2 and N_2 as function of temperature (thermogram) was generated at the end of the reaction. The results are presented in Fig. 5.

On the basis of the observed desorption of NH_3, it is concluded that the surface groups on δ-Al_2O_3 are acidic. Indeed, some water molecules are also present on the surface of the nanoparticles as seen by the TPD measurements, inspite of subjecting them to thorough drying at ∼110 °C for a few hours. As noted by Capiglia et al. [28] for a $(PEO)_8$–$LiClO_4$ system with SiO_2 nanoparticles fillers, the moisture on the surface of the particles has the effect of decreasing the ionic conductivity of the NCPE. The presence of the water molecules on the surface of δ-Al_2O_3 nanoparticles used in the present system, which could not be removed

even after drying, may have the effect of decreasing the conductivity in a similar way.

3.4. NMR studies

NMR is a powerful local probe of structure and dynamics of condensed matter and as such is used extensively in the study of solid electrolytes. The most useful information obtained by NMR in the case of SPEs is the identity of the mobile species, its dynamics and very often its interaction with the surroundings. Over the last few years, a number of NMR reports have been published in NCPEs [12,15,17,29–31]. Here again, there is no unanimity of either observations or interpretations, a fact that is indicative of the complexity of the phenomena occurring in these systems. It is generally expected that when ionic motion occurs, the NMR linewidth of the mobile nucleus decreases. In contrast, Dai et al. [29] with $(PEO)_{1.5}$ + LiI + nanoscale Al_2O_3 or MgO, Chung et al. [15] with $(PEO)_8$ + $LiClO_4$ + TiO_2 nanoparticles and Forsyth et al. [30] with 3PEG + $LiCLO_4$ + TiO_2, SiO_2 and Al_2O_3 nanoparticles, observed an increase in the ^{7}Li linewidth on addition of nanoparticles though the ionic conductivity increased. One possible explanation offered was that nanoparticles cause the Li–H distance to decrease and this results in an increase in the Li–H heteronuclear dipolar interaction which is shown to be the main contributor to the linewidth through ^{1}H decoupling experiments [17]. While this explanation is reasonable, Mustarelli et al. [12] with PEO_8 + $LiCLO_4$ or $LiN(CF_3SO_2)_2$ + nanoscale SiO_2 found a decrease in the ^{7}Li linewidth of nanocomposites. Bloise et al. [31] with PEO + $LiClO_4$ or $LiBF_4$ + α-Al_2O_3 or γ-Al_2O_3 observed mixed behavior in that γ-Al_2O_3 caused an increase in the linewidth while α-Al_2O_3 resulted in a decrease in the linewidth. It is clear that the behavior can be different in different systems and there is a need for more comprehensive studies before clear systematics emerge.

^{1}H and ^{7}Li NMR studies of the NCPE with a composition that corresponds to the maximum ionic conductivity, i.e., 10 mol% δ-Al_2O_3, were carried out on a Bruker DSX-300 spectrometer operating at frequencies of 300 and 117 MHz, respectively, in the temperature range of 250–340 K for ^{1}H and 225–340 K for ^{7}Li. A single 90° pulse of 4–5 μs was used with 5 s recycle delay. For the NMR experiments, the films were cut into narrow strips and filled into 5 mm glass tubes in a nitrogen atmosphere. The open end of the tube was closed using teflon tape. The samples in the tubes were kept in a glove box until the time of experiment.

The linewidth behavior of ^{1}H and ^{7}Li resonances are shown in Figs. 6 and 7 respectively for both undoped and doped samples. The inset (a) in Fig. 7 shows the actual ^{7}Li signals at room temperature. Two points are noteworthy with respect to these NMR results. First, on addition of the nanoparticles, the ^{7}Li linewidth *decreases* significantly while there is only a marginal decrease in the ^{1}H linewidth. The obvious inference is that there is very little effect of doping on the chain dynamics (but see below) while the ^{7}Li

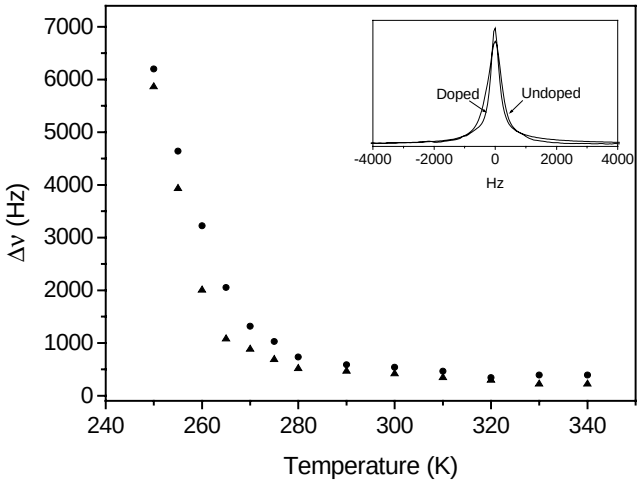

Fig. 6. ^{1}H linewidth vs. temperature plot for $(PEG)_{46}LiClO_4$ + δ-Al_2O_3 (10 mol%); circles and triangles represent the linewidths for the undoped and doped samples respectively. Inset shows ^{1}H signals at room temperature.

mobility has significantly increased. Second, the motional narrowing of both the resonances is sharper in the doped samples though the effect is more predominant in ^{7}Li resonance. This result is interesting in view of the fact that glass transition temperature T_g, which is associated with the onset of chain dynamic is practically unaffected by doping. The implication is that though the onset of the dynamics remains the same, the presence of the nanoparticles helps to accelerate the ^{7}Li dynamics. Standard procedures have been used to evaluate the motional parameters from the linewidth data. Using $\tau_c = (1/\alpha\pi\Delta\nu)\times\tan(\pi/2\times(\Delta\nu)^2-(\Delta\nu_r)^2/(\Delta\nu_d)^2-(\Delta\nu_r)^2)$ [32], where τ_c is the correlation time, α a parameter of order unity, $\Delta\nu$ the linewidth in the narrowing region (in Hz), $\Delta\nu_r$ the residual linewidth, and $\Delta\nu_d$ the rigid linewidth,

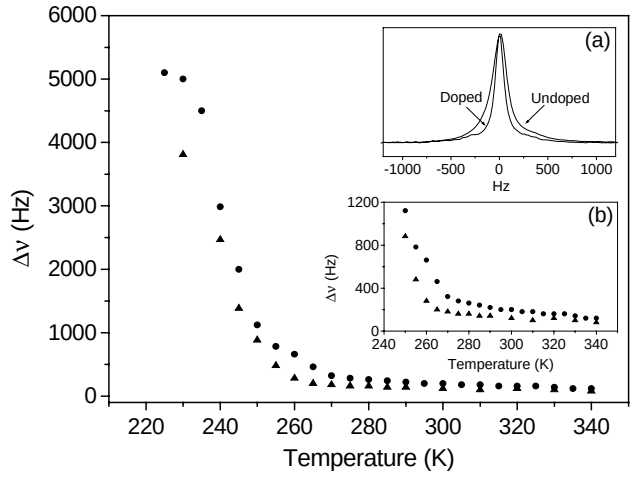

Fig. 7. ^{7}Li linewidth vs. temperature plot for $(PEG)_{46}LiClO_4$ + δ-Al_2O_3 (10 mol%); circles and triangle represent the linewidths for the undoped and doped samples respectively. Inset (a) shows ^{7}Li signals at room temperature. Inset (b) is expanded plot of main figure to show sharpness of the transition for doped sample.

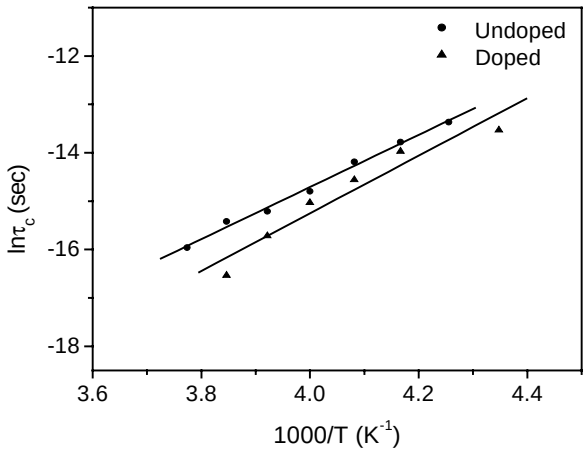

Fig. 8. Correlation time vs. temperature plot for undoped and doped $(PEG)_{46}LiClO_4 + \delta\text{-}Al_2O_3$ (10 mol%). Solid lines (—) are fits to correlation time equation: $\ln(\tau_c) = \ln(\tau_o) + (E_{aNMR}/1000\,k) \times 1000/T$.

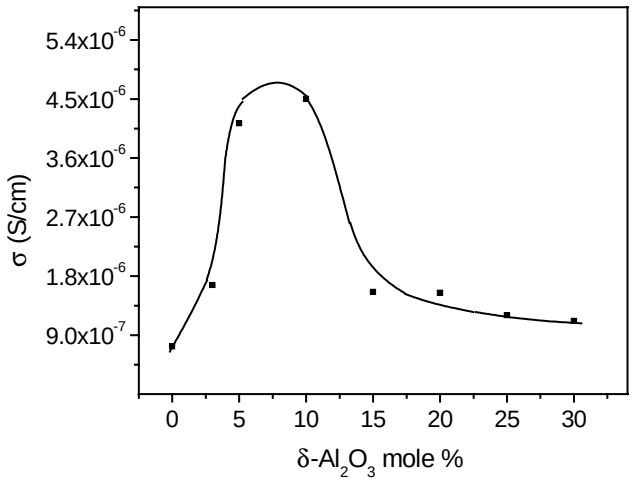

Fig. 9. Conductivity vs. $\delta\text{-}Al_2O_3$ (mol%) plot for $(PEG)_{46}LiClO_4 + \delta\text{-}Al_2O_3$ at 300 K. Solid line is a guide to the eye.

τ_c values are calculated at various temperatures and are shown in Fig. 8. The parameters E_a and τ_o are estimated from the slope of the plot. The ionic conductivity σ_{NMR} is also calculated employing the Nernst–Einstein relation $\sigma_{NMR} = Nq^2d^2/6\tau kT$, where N is the lithium concentration per unit volume, d the average ionic jump distance, and q the ionic charge. Considering an average Li–Li distance of ~4 Å, the value of N in $(PEG)_{46}LiClO_4$ can be calculated from the molecular weights and densities of PEG and $LiClO_4$, respectively. A value of $3.3 \times 10^{26}\,m^{-3}$ is obtained. The results are summarized in Table 2. Two interesting points emerge from the data. First, the value of σ_{NMR} in the doped sample is higher, which is consistent with the conductivity measurements (see below). The actual magnitude obtained by NMR measurements is higher by more than an order of magnitude. This could be because of the sensitivity of NMR to local dynamics in contrast with conductivity measurement, which measures only the long-range transport. Another reason for this differences could be that while conductivity measurement responds to the motion of only charged (i.e., dissociated) species, NMR can sense the motion of undissociated molecules as well. Such differences in the σ determined by the two techniques have been discussed earlier [33]. The second interesting observation from the data in Table 2 is that the activation energy E_{aNMR} increases slightly on doping. Therefore, the conductivity enhancement is mostly due to an increase in the attempt frequency in a way similar to the observations of Mustarelli et al. [12].

3.5. Ionic conductivity

The variation of ionic conductivity, σ, with content of $\delta\text{-}Al_2O_3$ nanoparticles is presented in Fig. 9. It is observed that starting from a value of $7.3 \times 10^{-7}\,S\,cm^{-1}$ for no filler content, the conductivity goes on increasing, reaches a maximum of $\sim 4.5 \times 10^{-6}\,S\,cm^{-1}$ around 10 mol% filler before decreasing again. While this general behavior is typical of NCPEs [34], it must be noted that the maximum enhancement observed of nearly one order is quit significant. Except for a couple of studies [35,36], most other authors report an enhancement by a few times in the conductivity on the introduction of nanoparticles [13,37].

The decrease with increasing filler content after the peak value is understood in terms of the increasing blocking effect of the conduction pathways by the electrically insulating nanoparticles. The initial increase for low filler content, in principle, can have different origins: (i) increased segmental motion of the host polymer [10], (ii) an increase in the number of charge carriers [4,12], or (iii) an increase in the mobility of the charge carriers [12,14]. A combined analysis of the above DSC and NMR studies enables the following mechanism to be proposed for the enhancement in σ. It is noted that there is no appreciable change in T_g in the doped samples. The ^1H NMR linewidth also does not undergo any significant narrowing. Therefore, it is concluded that the segmental motion remains unaffected by the filler. As seen in Fig. 4, however, there is a sharp decrease in the percentage crystallinity of the sample from ~70% down to about 62% for

Table 2
Results of NMR parameters obtained from ^7Li linewidths for $(PEG)_{46}LiClO_4 + \delta\text{-}Al_2O_3$ (10 mol%) system

Sample	τ_o (s)	E_{aNMR} (eV)	τ_c (s) at 300 K	σ_{NMR} ($S\,cm^{-1}$)	σ ($S\,cm^{-1}$)
Undoped	1.83×10^{-16}	0.46	1.13×10^{-8}	1.3×10^{-5}	7.27×10^{-7}
Doped	1.11×10^{-17}	0.51	4.5×10^{-9}	4.158×10^{-5}	4.503×10^{-6}

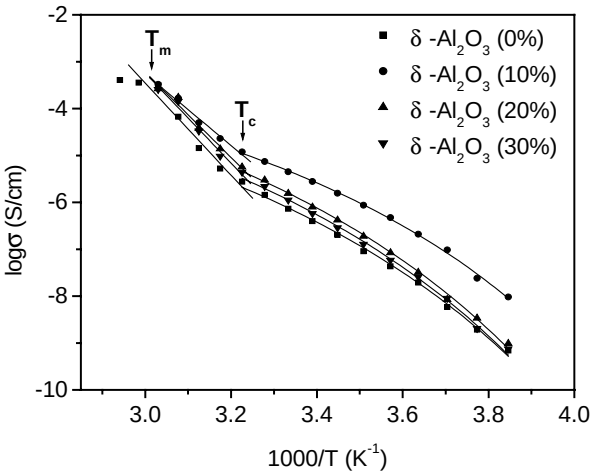

Fig. 10. Conductivity vs. temperature plot for $(PEG)_{46}LiClO_4 + \delta\text{-}Al_2O_3$. Solid lines are fits to Arrhenius (above T_c) and VTF (below T_c) equations.

10 mol% nanoparticles. Simultaneously, there is a narrowing of the ^{7}Li signals that indicates an increase in the mobility of ^{7}Li nuclei. Thus, the conductivity enhancement is caused by an increase in the amorphous fraction of the sample accompanied by an increase in the mobility of the Li ions.

How does the introduction of the nanoparticles lead to these effects? Croce et al. [13] and Jayathilaka et al. [14] have considered the nanoparticles–SPE interaction in detail. It was observed that the nature of the interaction and the consequent effect on conductivity was sensitively dependent on whether the surface groups of the nanoparticles are acidic, basic or neutral. The TPD studies have shown that the surface groups on the $\delta\text{-}Al_2O_3$ particles used here are acidic. These acidic groups would interact with ClO_4^- anions as well as with PEG segments, which results in an increase in the salt dissociation and in the local PEG amorphous fraction [4]. Both these effects contribute to the enhancement of the ionic conductivity through an increase in the number of charge carriers. Additionally, the NMR results indicate an increase in the ionic mobility since narrower linewidths are observed in $\delta\text{-}Al_2O_3$ doped samples compared with the undoped one.

As mentioned earlier, two contrasting effects of nanoparticle doping on ^{7}Li NMR linewidths have been reported. Obviously, the result is system specific, namely: some systems show an increase in the linewidth while certain other systems show the opposite effect. The understanding of the specific nature of the system causing these opposite effects requires further investigation.

Conductivity versus temperature plots for the $(PEG)_{46}LiClO_4 + \delta\text{-}Al_2O_3$ system are presented in Fig. 10. The conductivity increases monotonically as the temperature rises. The plots show that there exists a temperature T_c below which the conductivity plot has a curvature and above which it linearly and steeply rises up to the melting temperature (≈330 K), as found with earlier observations [38,39]. The region below T_c fits the VTF equation ($\sigma = A/T^{1/2} \exp[-B/k(T - T_o)]$ [40] where A, B and T_o are treated as fitting parameters with the values listed in Table 3. T_o is usually 30–50 °C below T_g and is called the equilibrium glass transition temperature [41]. An increase in T_o is observed on dispersal of the nanoparticles filler. The Arrhenius equation ($\sigma = \sigma_0 \exp[-E_a/kT]$, where symbols have their usual meanings) fits the region above T_c. The cross-over between Arrhenius and VTF behavior of $\sigma(T)$ has been reported widely and discussed in literature [38]. This behavior is rationalized by arguing that since VTF dependence is governed by the energy interval $(T - T_o)$ and the Arrhenius dependence by the temperature T, for $T \gg T_o$ the two should merge. A considerable amount of modeling effort has been devoted to understanding this behavior in terms of the free volume theory of Cohen and Turnbull [42]. A detailed discussion regarding this cross-over has been reported previously [39]. The activation energy E_a decreases as the mol% of nanoparticles increases and then shows a minimum at the concentration that shows the maximum ionic conductivity (Table 3).

Table 3
Arrhenius and VTF parameters for $(PEG)_{46}LiClO_4 + \delta\text{-}Al_2O_3$

Mol%	E_a (eV)	T_c (K)	A (S K$^{1/2}$ cm^{-1})	B (eV)	T_o (K)
0	2.04	310	1.79	0.11	195.75
10	1.58	310	1.50	0.09	198.03
20	1.88	310	5.58	0.11	196.63
30	1.99	310	4.42	0.12	195.83

4. Conclusions

The effect of the dispersion of $\delta\text{-}Al_2O_3$ nanoparticles on the ionic conductivity of $(PEG)_{46}LiClO_4$ polymer electrolyte has been examined. An enhancement in ionic conductivity by nearly one order of magnitude is observed at 10 mol% nanoparticles. The conductivity goes through a maximum as a function of the content of nanoparticles in the SPE. A decrease in the degree of crystallinity is observed on doping with nanoparticles in the SPE while the glass transition temperature T_g and the melting temperature T_m remain essentially unchanged. ^{7}Li NMR motional narrowing points to an increase in the effective mobility of the lithium ions on doping with nanoparticles. The activation energy is the lowest at 10 mol%, i.e., for the composition that shows the maximum ionic conductivity. The enhancement in the ionic conductivity of $(PEG)_{46}LiClO_4 + \delta\text{-}Al_2O_3$ system is attributed to a reduction in the degree of crystallinity, a decrease in the activation energy, and an increase in the effective mobility of ions.

Acknowledgements

The authors are grateful to the University Grant Commission, Govt. of India for financial support. Thanks are

also due to Prof. M.S. Hegde, SSCU for the TPD experiment, and to Nanopowder Enterprises Inc., USA for a gift of the nanoparticles. One of the authors (Th. Joykumar Singh) acknowledges the Council of Scientific and Industrial Research, New Delhi, for a fellowship.

References

[1] F.M. Gray, Solid Polymer Electrolyte—Fundamentals and Technological Applications, VCH, New York, 1991.
[2] J.E. Weston, B.C.H. Steele, Solid State Ionics 7 (1982) 75.
[3] W. Wieczorek, Z. Florjańczyk, J.R. Stevens, Electrochim. Acta 40 (1995) 2251.
[4] F. Croce, G.B. Appetechi, L. Persi, B. Scrosati, Nature 394 (1998) 456.
[5] J. Przyuski, K. Such, H. Wycilik, W. Wieczorek, Synth. Met. 35 (1990) 241.
[6] N. Munichandraiah, L.O. Scanlon, R.A. Marsh, J. Appl. Electrochem. 25 (1995) 857.
[7] F. Capuano, F. Croce, B. Scrosati, J. Electrochem. Soc. 138 (1991) 1918.
[8] H.Y. Sun, H.-J. Sohn, O. Yamamoto, Y. Takeda, N. Imanishi, J. Electrochem. Soc. 146 (1999) 1672.
[9] W. Krawiec, L.O. Scanlon Jr., J.P. Feller, R.A. Vaia, S. Vasudevan, E.P. Giannelis, J. Power Sources 54 (1995) 310.
[10] Y.W. Kim, W. Lee, B.K. Choi, Electrochim. Acta 45 (2000) 1473.
[11] C. Capiglia, P. Mustarelli, E. Quartarone, C. Tomasi, A. Magistris, Solid State Ionics 118 (1999) 73.
[12] P. Mustarelli, C. Capiglia, E. Quartarone, C. Tomasi, P. Ferloni, Phys. Rev. B 60 (1999) 7228.
[13] F. Croce, L. Persi, B. Scrosati, F. S-Fiory, E. Plichta, M.A. Hendrickson, Electrochim. Acta 46 (2001) 2457.
[14] P.A.R.D. Jayathilaka, M.A.K.L. Dissanayake, I. Albinsson, B.E. Mellander, Electrochim. Acta 47 (2002) 3257.
[15] S.H. Chung, Y. Wang, S.G. Greenbaum, M. Marcinek, L. Persi, F. Croce, W. Wieczorek, B. Scrosati, J. Phys.: Condens. Matter 13 (2001) 11763.
[16] A.S. Best, J. Adebahr, P. Jacobsson, D.R. MacFarlane, M. Fosyth, Macromolecules 34 (2001) 4549.
[17] C.C. Tambelli, A.C. Bloise, A.V. Rosário, E.C. Pereira, C.J. Magon, J.P. Donoso, Electrochim. Acta 47 (2002) 1677.
[18] J. Shi, C.A. Vincent, Solid State Ionics 60 (1993) 11.
[19] M. Marcinek, A. Bac, P. Lipka, A. Zaleska, G. Ukowska, R. Borkowska, W. Wieczorek, J. Phys. Chem. B 104 (2000) 11088.
[20] Th.J. Singh, S.V. Bhat, Bull. Mater. Sci. 26 (2003) 707.
[21] B.A. Boukamp, Equivalent Circuit Software (EQUIVCRT.PAS) Ver. 3.39, University of Twente, Enschede, The Netherlands, 1989.
[22] P.S. Santos, H.S. Santos, S.P. Toledo, Mater. Res. 3 (2000) 104.
[23] A. Roy, A.K. Sood, Pramana 44 (1995) 201.
[24] A. Günier, X-Ray Diffraction in Crystals, Imperfect Crystals and Amorphous Bodies, W.H. Freeman, San Francisco, 1963, Chapter 5, p. 121.
[25] H.P. Klug, L.E. Alexander, X-Ray Diffraction Procedures for Polycrystalline and Amorphous Materials, Wiley, New York, 1973, pp. 635, 687.
[26] Th.J. Singh, T. Mimani, K.C. Patil, S.V. Bhat, Solid State Ionics 154–155 (2002) 21.
[27] D. Fauteux, in: J.R. MacCallum, C.A. Vincent (Eds.), Polymer Electrolyte Reviews, vol. 2, Elsevier, London, 1989, p. 137.
[28] C. Capiglia, P. Mustarelli, E. Quartarone, C. Tomasi, A. Magistris, Solid State Ionics 118 (1999) 73.
[29] Y. Dai, Y. Wang, S.G. Greenbaum, S.A. Bajue, D. Golodnitsky, G. Ardel, E. Straus, E. Peled, Electrochim. Acta 43 (1998) 1557.
[30] M. Forsyth, D.R. MacFarlane, A. Best, J. Adebahr, P. Jacobsson, A.J. Hill, Solid State Ionics 147 (2002) 203.
[31] A.C. Bloise, C.C. Tambelli, R.W.A. Franco, J.P. Donoso, C.J. Magon, M.F. Souza, A.V. Rosario, E.C. Rereira, Electrochim. Acta 46 (2001) 1571.
[32] J.R. Hendrickson, P.J. Bray, J. Magn. Res. 9 (1973) 341.
[33] D. Brinkmann, Prog. NMR Spectrosc. 24 (1992) 527.
[34] B.K. Choi, K.H. Shin, Solid State Ionics 86–88 (1996) 303.
[35] N. Munichandraiah, B. Kumar, S. Rodrigues, J. Power Sources 111 (2002) 165.
[36] S.H. Chung, Y. Wang, L. Persi, F. Croce, S.G. Greenbaum, B. Scrosati, E. Plichta, J. Power Sources 97–98 (2001) 644.
[37] B. Kumar, J.D. Schaffer, N. Munichandraiah, L.G. Scanlon, J. Power Sources 47 (1994) 63.
[38] M.A. Ratner, in: J.R. MacCallum, C.A. Vincent (Eds.), Polymer Electrolyte Reviews, vol. 1, Elsevier, London, 1987, p. 185.
[39] N. Binesh, S.V. Bhat, J. Polym. Sci. Part B: Phys. 36 (1998) 1201.
[40] H. Vogel, Phys. Z. 22 (1921) 645;
V.G. Tamman, H.Z. Hesse, Anorg. Allg. Chem. 19 (1926) 245;
G.H. Fulcher, J. Am. Ceram. Soc. 8 (1925) 339.
[41] J.H. Gibbs, E.A. DiMarzio, J. Chem. Phys. 28 (1958) 373.
[42] M.H. Cohen, D. Turnbull, J. Chem. Phys. 31 (1959) 1164.